Electronic Research Archive

https://www.aimspress.com/journal/era

ERA, 34(4): 2194–2221.
DOI: 10.3934/era.2026099
Received: 21 November 2025
Revised: 01 March 2026
Accepted: 05 March 2026
Published: 11 March 2026

Research article

A bio-inspired learning-and-reusing control strategy for multi-zone HVAC systems

Suna Wang[1], Zhaohui Qi[2,*], Haiqun Chen[3,*], Lu Sun[4] and Haotian Shi[5]

[1] Department of Infrastructure, Sun Yat-Sen Memorial Hospital of Sun Yat-Sen University, Guangzhou 510120, China

[2] School of Energy Science and Engineering, Central South University, Changsha 410083, China

[3] School of Mechanical and Electrical Engineering, Guangzhou University, Guangzhou 510006, China

[4] School of Electrical and Automation Engineering, Nanjing Normal University, Nanjing 210023, China

[5] School of Electronics and Communication Engineering, Guangzhou University, Guangzhou 510006, China

* **Correspondence:** Email: 700002@csu.edu.cn, 2112307025@e.gzhu.edu.cn.

Abstract: Heating, ventilation, and air conditioning (HVAC) systems are a major contributor to global building energy consumption; however, their control is complicated by inherent parametric uncertainties and time-varying disturbances. To address the limitations of conventional methods, a novel two-stage "learning-and-reusing" framework was proposed, which fundamentally differs from existing methods by: (i) decoupling parameter learning from disturbance rejection to avoid the single-stage trade-off; (ii) using concurrent learning and an estimator for parameter identification under relaxed excitation conditions and input saturation. In the first learning stage, a concurrent-learning-based adaptive controller accurately identifies key thermodynamic parameters, such as the heat transfer coefficient and the cross-sectional areas of the wall, while simultaneously maintaining precise temperature regulation, thereby building a reliable knowledge base. In the second reusing stage, the identified model is used within a disturbance observer-based robust controller to precisely compensate for time-varying disturbances, such as fluctuating solar radiation and internal heat loads. Simulations on multi-zone building models validated the framework, demonstrating successful parameter convergence and superior robust tracking performance compared to conventional methods. This work offers an efficient, bio-inspired solution for intelligent building thermal management.

Keywords: heating, ventilation, and air conditioning systems; learning control; adaptive control; disturbance observer; nonlinear systems

1. Introduction

The building sector is a significant contributor to global energy consumption, largely due to the operation of heating, ventilation, and air conditioning (HVAC) systems for maintaining indoor thermal comfort [1, 2]. In the context of growing emphasis on energy efficiency and carbon neutrality, advanced control strategies for building thermal management have become a focal point of research. The primary objective is to regulate indoor temperatures to meet occupant comfort requirements while minimizing energy usage–a challenging task due to the complex, nonlinear, and uncertain nature of building thermodynamic relationships [3]. To address the challenges in HVAC control, various methodologies have been developed spanning different control paradigms. Model predictive control (MPC) [4] has gained significant attention for its ability to explicitly handle system constraints and optimize energy usage through forecasting. However, the accuracy of the model, disturbances, and weather forecasting all affect the energy consumption and performance of MPC [5]. A more fundamental challenge is that key thermodynamic parameters, such as thermal conductance of building envelopes and internal heat gains from occupants and equipment, are often difficult to identify accurately and can vary across different environments, significantly increasing the controller's design complexity and implementation cost [6]. The work in [7] presents a dynamic HVAC model comprising thermal zones, coils, and ductwork, and develops a proportional integral derivative (PID) control strategy to maintain indoor comfort while reducing energy consumption. The study applies Ziegler-Nichols tuning to optimize controller parameters, demonstrating effective disturbance rejection in simulations. Nevertheless, the control performance exhibits significant sensitivity to these parameters, requiring careful gain adjustments to achieve satisfactory responses.

Given the limitations of conventional methods, recent research has witnessed a paradigm shift toward hybrid methodologies that synergize classical control [8–10] with intelligent learning techniques [11–13]. The work in [14] combines the PID controller with a deep reinforcement learning algorithm, and proposes a method for optimizing PID parameters to control the indoor temperature of tomato-planted greenhouses. Tests show this method outperforms on/off and Ziegler-Nichols-tuned PID controllers in energy efficiency and crop temperature maintenance. The work in [15] combines artificial neural networks with a search algorithm, and proposes a new optimal operation strategy for the HVAC system in commercial buildings, where neural networks conduct repeated online learning to mitigate overfitting after initiating optimal scheduling. The work in [16] combines an integrated neural network prediction model for indoor environmental quality with an optimizing control, and proposes an intelligent HVAC-integrated control strategy for school buildings, which addresses the need to improve the indoor environment and reduce energy consumption. On the other hand, building thermal dynamics are subject to time-varying disturbances [17, 18], including fluctuating solar irradiance, varying occupancy patterns, and changing outdoor weather conditions. These disturbances [19], if not properly compensated for, can lead to poor temperature regulation and increased energy consumption. To address this issue, the work in [20] incorporates a bias compensation mechanism and integral action into the Q-learning framework, eliminating the requirement to measure or manipulate disturbances while avoiding disturbance-induced bias in optimal control estimates.

The integration of cooperative control methodologies [21–24] becomes particularly crucial when addressing the complexities of multi-zone HVAC systems. These systems present additional challenges due to their inherent thermal coupling between zones and the need for coordinated control across

multiple indoor units sharing limited refrigerant flow. In [25], by combining online adaptive learning with information exchange between neighboring zones, a distributed adaptive control scheme for multi-zone HVAC systems in buildings with multiple climate zones is proposed. Each zone's controller achieves local temperature control by compensating for neighboring zones' effects and system parameter changes, while real-time estimating interconnection parameters to improve control accuracy. In [26], integrating a modified distributed model with predictive control, a local cooling cost, and an air-mass-rate penalty with a multi-layer framework, a coordinated control strategy for a multi-zone HVAC is developed, and the effectiveness of this strategy is verified through simulation. In [27], a novel optimal control method for multi-zone HVAC systems is proposed using reinforcement learning and active disturbance rejection control via a main-auxiliary controller configuration, addressing noise and disturbances that affect control accuracy and computational challenges posed by multiple variables. In [28], a hierarchical distributed control for multi-evaporator AC systems is proposed, integrating upper-layer open-loop optimization with lower-layer distributed model predictive control to minimize energy cost while maintaining comfort. In [29], a fast power dispatch model is developed for a multi-zone HVAC using Wasserstein-distance-based distributionally robust chance-constrained optimization to handle uncertainties from forecasting errors.

Despite these advancements, effectively managing both parametric uncertainties and time-varying disturbances while maintaining system stability continues to present a significant research challenge in HVAC control. Existing learning-based solutions for HVAC control still face two predominant challenges. On one hand, many data-driven approaches require massive datasets for offline training and substantial computational resources, posing significant barriers to their practical deployment in commercial HVAC systems. For instance, [30] focuses on energy optimization of CO_2 heat pump systems but does not address online identification, while [31] proposes a bi-level optimal control for a multi-zone DOAS-assisted HVAC but relies on known models. In [32], by using the Taylor-based linearization system, a hierarchical control strategy optimizing comfort and energy for air conditioning systems with uncertain parameters is proposed. On the other hand, certain online learning strategies, such as conventional adaptive control [33–35], can adjust controller parameters in real-time to maintain system performance but often lack guaranteed convergence to the true physical parameters of the system. This inherent limitation (wherein control is achieved without genuine system identification) prevents the controller from truly learning the model knowledge from operational data, thereby failing to emulate the bio-inspired learning capability of "learning from past experiences and reusing the experiences to improve control performance" [36, 37]. Consequently, the core difficulty addressed in this work lies in designing a control framework that seamlessly integrates both learning and application. The primary challenges are twofold: first, to enable accurate online identification of unknown constant system parameters under relaxed conditions that do not rely on persistent excitation (PE) [38, 39] and input saturation constraints [40], thereby building a valuable knowledge base or experience; and second, to leverage this identified model knowledge to construct a high-performance controller robust against time-varying disturbances. To bridge this gap, this paper proposes a novel two-stage learning control framework for multi-zone HVAC systems. In the first "learning" stage (imitating humans in learning knowledge from the experience), the controller focuses on accurately identifying the unknown constant parameters of the building's thermal model. In the second "reusing" stage (reusing knowledge to enhance performance), the controller utilizes the identified model to achieve robust performance against time-varying disturbances. The main contributions of this work are twofold:

- In contrast to conventional adaptive control methods, this paper proposes a novel two-stage control framework. This framework achieves precise parameter estimation under relaxed excitation conditions, through a synergistic integration of concurrent learning and a disturbance observer. This integration enables robust compensation for time-varying disturbances.
- To achieve accurate identification of parameters under input saturation constraints, this paper constructs an adaptive update law based on prediction error. Both comprehensive Lyapunov-based stability theoretical analysis and comparison simulations validate the framework's theoretical robustness and practical effectiveness.

The remainder of this paper is organized as follows. Section 2 describes the multi-area building thermodynamic model and formulates the control problem. Section 3 details the design and stability analysis of the two-stage control method, including the concurrent-learning-based adaptive control in Stage 1 and the disturbance observer-based robust control in Stage 2. Section 4 presents simulation results to validate the proposed approach. Finally, Section 5 concludes the paper. The main symbols used throughout the paper are as shown in Table 1.

Table 1. Summary of symbols used throughout the paper.

Parameter	Symbol
Thermal capacitance	C_{zi}
Exterior wall heat transfer coefficient	U_{wall}
Interior wall heat transfer coefficient	U_{wallin}
Window heat transfer coefficient	U_{win}
Outdoor wall area	$A_{\text{out},i}$
Window area	$A_{\text{win},i}$
Adjacent wall area	$A_{\text{w},i,j}$
Internal heat load	$Q_{\text{in,s},i}$
Solar heat gain coefficient	α_{SHGC}
Solar radiation intensity	I
Specific heat capacity of air	c
Air density	ρ
Wind speed	v
Intake port area	F
Lumped parameter for exterior gains	θ_{i1}
Lumped parameter for solar+internal gains	θ_{i2}
Thermal coupling parameter (zone j to i)	ϑ_{ij}
Regressors for θ_{i1}, θ_{i2}	ϕ_{i1}, ϕ_{i2}
Regressor for the coupling term	φ_{ij}
Tracking error	e_i
Tracking error estimation	$\hat{e}_i$
Prediction error	$\tilde{e}_i$

2. Problem description

For the i-th zone of multi-zone HVAC systems, the energy consumption of indoor temperature can be calculated through the following thermodynamic model [41]:

$$C_{zi}\frac{\mathrm{d}T_{zi}}{\mathrm{d}t} = Q_{\mathrm{out},i} + \sum_{j\in N_i} Q_{\mathrm{w},i,j} + Q_{\mathrm{win},i} + Q_{\mathrm{air},i} + Q_{\mathrm{in,s},i} - Q_{\mathrm{e,s},i} \tag{2.1}$$

where T_{zi} stands for the indoor temperature of the i-th area; C_{zi} is the thermal capacitance of the i-th area; $Q_{\mathrm{out},i}$ is the heat transfer through the wall; $Q_{\mathrm{w},i,j}$ is the heat transferred from the adjacent area j to area i; N_i is the set of areas that have a thermal influence on area i; $Q_{\mathrm{win},i}$ is the heat transferred to area i through the windows; $Q_{\mathrm{air},i}$ is the heat penetrating from the outdoor air; $Q_{\mathrm{in,s},i}$ is the total internal heat load of area i, which is related with the latent heat load transferred from indoor people, lighting, and office equipment; $Q_{\mathrm{e,s},i}$ is the reasonable cooling load of area i.

The heat transfer through the wall $Q_{\mathrm{out},i}$, the heat transfer through the adjacent area $Q_{\mathrm{w},i,j}$, the heat transfer through the windows $Q_{\mathrm{win},i}$, and the heat penetrating from the outdoor air $Q_{\mathrm{air},i}$ can be represented as:

$$Q_{\mathrm{out},i} = U_{\mathrm{wall}}A_{\mathrm{out},i}(T_{\mathrm{out}} - T_{zi}) \tag{2.2}$$

$$Q_{\mathrm{w},i,j} = U_{\mathrm{wallin}}A_{\mathrm{w},i,j}(T_{zj} - T_{zi}) \tag{2.3}$$

$$Q_{\mathrm{win},i} = A_{\mathrm{win},i}(\alpha_{\mathrm{SHGC}}I + U_{\mathrm{win}}(T_{\mathrm{out}} - T_{zi})) \tag{2.4}$$

$$Q_{\mathrm{air},i} = cpvF(T_{\mathrm{out}} - T_{zi}) \tag{2.5}$$

$$Q_{\mathrm{e,s},i} = E_i\mathrm{sat}(P_i) \tag{2.6}$$

where U_{wall} stands for the heat transfer coefficient of the exterior wall, U_{wallin} stands for the heat transfer coefficient of the interior wall, U_{win} stands for the area of the window, $A_{\mathrm{out},i}$ is the cross-sectional area of the outdoor wall, $A_{\mathrm{w},i,j}$ is the cross-sectional area of the indoor wall, T_{out} is the outdoor temperature, T_{zj} is the temperature of the adjacent area j, α_{SHGC} is the solar heat gain coefficient, I is the intensity of solar radiation, c represents the specific heat capacity of air, p represents the air density, v represents the wind speed, and F represents the area of the intake port. In this paper, we assume the heat transfer coefficients U_{wall}, U_{wallin}, and U_{win} of the exterior wall, interior wall, and window, the cross-sectional areas of the outdoor wall $A_{\mathrm{out},i}$ and the indoor wall $A_{\mathrm{w},i,j}$, and the coefficients $\alpha_{\mathrm{SHGC}}, I, c, p, v, F$ are unknown constants, E_i is the energy efficiency ratio of the air conditioning system within region i, P_i is the cooling power of the air conditioning system in area i, and sat$(\cdot)$ stands for the saturation function, which is used to simulate the upper limit of the cooling power of an actual air conditioner.

The purpose of the air conditioner is to provide the reasonable cooling power P_i, which keeps the temperature at the value set by the user. In practice, the power of the air conditioner is limited, so the cooling power P_i is limited by the saturation function sat$(\cdot)$:

$$\mathrm{sat}(P_i) = \begin{cases} P_{i,\max}, & P_i > P_{i,\max} \\ P_i, & P_{i,\min} \le P_i \le P_{i,\max} \\ P_{i,\min}, & P_i < P_{i,\min} \end{cases} \tag{2.7}$$

where $P_{i,\max}$ and $P_{i,\min}$ are the known upper and lower bounds of the heat provided by the i-th air conditioner.

Control objective: The goal of this paper is to design a two-stage control scheme for the thermodynamic model (2.1).

- Stage 1 (learning knowledge from the experience): An adaptive controller will be designed not only to stabilize the temperatures but also to accurately identify the unknown constant parameters (e.g., heat transfer coefficients, internal gains). This stage builds a "knowledge base" of the building's thermal dynamics under relaxed excitation conditions by leveraging historical data in a concurrent learning framework.
- Stage 2 (reusing knowledge to enhance performance): Utilizing the identified parameters from Stage 1 as a fixed nominal model, the objective shifts to robust tracking performance under time-varying uncertainties. A disturbance observer will be integrated into the control law to estimate and actively compensate for the time-varying disturbances in real-time, ensuring high-performance operation despite modeling imperfections and external perturbations.

3. Two-stage learning control method design

This section delineates the design and stability analysis of the proposed two-stage control scheme.

3.1. Stage 1: Concurrent-learning-based adaptive control

3.1.1. Controller design

In Stage 1, we assume that the solar heat gain coefficient α_{SHGC}, the intensity of solar radiation I, and the total internal heat load $Q_{\text{in,s},i}$ are constants. The system dynamics (2.1) can be rewritten as:

$$\frac{dT_{zi}}{dt} = \frac{1}{C_{zi}}\left(\theta_{i1}\phi_{i1} + \theta_{i2}\phi_{i2} + \sum_{j\in N_i} a_{ij}\vartheta_{ij}\varphi_{ij} - E_i\text{sat}(P_i)\right) \tag{3.1}$$

where $\theta_{i1} = U_{\text{wall}}A_{\text{out},i} + A_{\text{win},i}U_{\text{win}} + cpvF$, $\theta_{i2} = A_{\text{win},i}\alpha_{\text{SHGC}}I + Q_{\text{in,s},i}$, $\phi_{i1} = T_{out} - T_{zi}$, $\phi_{i2} = 1$, $\vartheta_i = U_{\text{wallin}}[A_{w,i,1}, \cdots, A_{w,i,n}]^T$, $\varphi_i = [T_{z1} - T_{zi}, \cdots, T_{zn} - T_{zi}]^T$. Moreover, a_{ij} is an adjacency indicator: $a_{ij} = 1$ if area i and area j share a wall; otherwise $a_{ij} = 0$.

Remark 1. *The parameters θ_{i1} are related to the exterior wall, the interior wall, window, and air. These factors tend to remain constant for at least a certain period of time. However, the parameters θ_{i2} contain the solar heat gain coefficient α_{SHGC}, the intensity of solar radiation I, and the total internal heat load $Q_{\text{in,s},i}$, where the internal heat load may change due to factors such as variations in indoor occupants. Stage 1 assumes that the parameters θ_{i2} are constant, meaning that any slow variations are neglected or absorbed into the constant estimate. If significant time-varying disturbances occur during Stage 1, they will bias the parameter estimates. However, in Stage 2, the disturbance observer treats the difference between the true time-varying $\theta_{i2}(t)$ and the fixed nominal estimate $\bar{\theta}_{i2}$ as part of the lumped disturbance $d_i(t)$, and compensates for it. We also provide a detailed analysis in the Simulation section.*

Let the desired indoor temperature be $T_{zi,d}(t)$. Define the tracking error: $e_i = T_{zi} - T_{zi,d}$. Differentiating tracking error e_i yields

$$\dot{e}_i = \frac{1}{C_{zi}}\left[\theta_{i1}\phi_{i1} + \theta_{i2}\phi_{i2} + \sum_{j\in N_i} a_{ij}\vartheta_{ij}\varphi_{ij} - E_i\text{sat}(P_i) - C_{zi}\dot{T}_{zi,d}\right]. \tag{3.2}$$

The control input P_i can be designed as

$$P_i = \frac{1}{E_i}\Big(\hat{\theta}_{i1}\phi_{i1} + \hat{\theta}_{i2}\phi_{i2} + \sum_{j\in N_i} a_{ij}\hat{\vartheta}_{ij}\varphi_{ij} - C_{zi}\dot{T}_{zi,d} + K_{i1}e_i\Big) \tag{3.3}$$

where $K_{i1} > 0$ is a feedback gain, and $\hat{\theta}_{i1}, \hat{\theta}_{i2}, \hat{\vartheta}_{ij}$ are parameter estimates.

Substituting (3.3) into the error dynamics (3.2), one has

$$\begin{aligned}\dot{e}_i =& \frac{1}{C_{zi}}\left[\theta_{i1}\phi_{i1} + \theta_{i2}\phi_{i2} + \sum_{j\in N_i} a_{ij}\vartheta_{ij}\varphi_{ij} - E_iP_i + E_iP_i - E_i\mathrm{sat}(P_i) - C_{zi}\dot{T}_{zi,d}\right]\\ =& \frac{1}{C_{zi}}\left[-K_{i1}e_i - \tilde{\theta}_{i1}\phi_{i1} - \tilde{\theta}_{i2}\phi_{i2} - \sum_{j\in N_i} a_{ij}\tilde{\vartheta}_{ij}\varphi_{ij} + \Delta(P_i)\right]\end{aligned} \tag{3.4}$$

where $\tilde{\theta}_{i1} = \theta_{i1} - \hat{\theta}_{i1}$, $\tilde{\theta}_{i2} = \theta_{i2} - \hat{\theta}_{i2}$, $\tilde{\vartheta}_{ij} = \vartheta_{ij} - \hat{\vartheta}_{ij}$, and $\Delta(P_i) = E_iP_i - E_i\mathrm{sat}(P_i)$ with $|\Delta(P_i)| \le \bar{\Delta}_i$.

Next, a system estimator to estimate e_i can be designed as

$$\begin{aligned}\dot{\hat{e}}_i =& \frac{1}{C_{zi}}\left[-K_{i2}(\hat{e}_i - e_i) + \hat{\theta}_{i1}\phi_{i1} + \hat{\theta}_{i2}\phi_{i2} + \sum_{j\in N_i} a_{ij}\hat{\vartheta}_{ij}\varphi_{ij} - E_iP_i + \Delta(P_i) - C_{zi}\dot{T}_{zi,d}\right]\\ =& \frac{1}{C_{zi}}\left[-K_{i2}(\hat{e}_i - e_i) - K_{i1}e_i + \Delta(P_i)\right]\end{aligned} \tag{3.5}$$

where $\hat{e}_i$ is the tracking error estimation. Then, defining the prediction error $\tilde{e}_i = \hat{e}_i - e_i$, we have

$$\begin{aligned}\dot{\tilde{e}}_i =& \frac{1}{C_{zi}}\left[-K_{i2}(\hat{e}_i - e_i) + \hat{\theta}_{i1}\phi_{i1} + \hat{\theta}_{i2}\phi_{i2} + \sum_{j\in N_i} a_{ij}\hat{\vartheta}_{ij}\varphi_{ij} - E_iP_i + \Delta(P_i) - C_{zi}\dot{T}_{zi,d}\right] - \dot{e}_i\\ =& \frac{1}{C_{zi}}\left[-K_{i2}\tilde{e}_i + (\tilde{\theta}_{i1}\phi_{i1} + \tilde{\theta}_{i2}\phi_{i2} + \sum_{j\in N_i} a_{ij}\tilde{\vartheta}_{ij}\varphi_{ij})\right]\end{aligned} \tag{3.6}$$

where $\dot{e}_i$ can be observed via filters or numerical differentiation methods in practice. Define historical prediction error π_i as

$$\begin{aligned}\pi_i(\tau) =& \left[\hat{\theta}_{i1}(t)\phi_{i1}(\tau) + \hat{\theta}_{i2}(t)\phi_{i2}(\tau) + \sum_{j\in N_i} a_{ij}\hat{\vartheta}_{ij}(t)\varphi_{ij}(\tau) - E_iP_i(\tau) + \Delta(E_iP_i(\tau))\right]\\ &- C_{zi}\dot{T}_{zi,d}(\tau) - C_{zi}\dot{e}_i(\tau).\end{aligned} \tag{3.7}$$

Substituting (3.2) into (3.7), we have

$$\begin{aligned}\pi_i(\tau) =& \left[\tilde{\theta}_{i1}(t)\phi_{i1}(\tau) + \tilde{\theta}_{i2}(t)\phi_{i2}(\tau) + \sum_{j\in N_i} a_{ij}\tilde{\vartheta}_{ij}(t)\varphi_{ij}(\tau)\right]\\ =& \left[\tilde{\theta}_{i1}(t), \tilde{\theta}_{i2}(t), \tilde{\vartheta}_i^T(t)\right]^T\left[\phi_{i1}(\tau), \phi_{i2}(\tau), \varphi_i^T(\tau)\right]\\ =& \tilde{\Theta}_i^T(t)\Phi_i(\tau).\end{aligned} \tag{3.8}$$

To accelerate parameter convergence, we construct the parameter update law to include a historical data term:

$$\dot{\hat{\Theta}}_i = -\rho_i \left(\tilde{e}_i \Phi_i + \epsilon_i \int_{t-\tau_d}^{t} \Phi_i(\tau)\pi_i(\tau)d\tau \right) \tag{3.9}$$

where $\rho_i = \text{diag}[\rho_{i1}, \rho_{i2}, \varrho_{ij}]$, $\epsilon_i = \text{diag}[\epsilon_{i1}, \epsilon_{i2}, \varepsilon_{ij}]$, $\rho_{i1}, \rho_{i2}, \varrho_{ij}, \epsilon_{i1}, \epsilon_{i2}, \varepsilon_{ij} > 0$ are positive weighting factors. This requires storing data over a window $[t - \tau_d, t]$.

Remark 2. *The primary advantages of the designed parameter update law are manifested through two key features: namely, the use of historical data* $\int_{t-\tau_d}^{t} \Phi_i(\tau)\pi_i(\tau)d\tau$ *and the incorporation of the prediction error* $\tilde{e}_i$*. The historical data term* $\int_{t-\tau_d}^{t} \Phi_i(\tau)\pi_i(\tau)d\tau$ *is crucial for achieving parameter convergence under relaxed excitation conditions, and it does not require the classical PE condition on the regressor* $\Phi_i(t)$*.*

Remark 3. *Comparing with the existing saturated-based adaptive control strategies, the prediction error* $\tilde{e}_i$ *instead of the tracking error* e_i *is utilized to construct the parameter update law. It should be pointed out that if we use the tracking error* e_i *to update the parameters, then the error* $\Delta(P_i) = E_i P_i - E_i \text{sat}(P_i)$ *caused by the input saturation constraint will be incorporated into the parameter update. In this case, it will disrupt the convergence of the parameters to their true values. So, the design of the estimator avoids the saturation error caused by input saturation in the traditional parameter update law.*

3.1.2. Stability analysis

Theorem 1. *Consider the multi-zone thermal system dynamics given by* (3.1) *under the control law* (3.3) *and the parameter update law* (3.9)*. The system ensures that all signals in the closed-loop system are uniformly ultimately bounded, and the tracking error* e_i *and the prediction error* $\tilde{e}_i$ *can be driven to a small residual set by an appropriate choice of the controller gains. Moreover, the prediction error* $\tilde{\Theta}_i$ *can converge to a small neighborhood of 0 if the stored historical data is sufficiently rich such that the matrix* $\Omega_i(t) = \int_{t-\tau_d}^{t} \Phi_i(\tau)\Phi_i^T(\tau)\, d\tau$ *satisfies* $\lambda_{\min}(\Omega_i(t)) \geq \underline{\lambda}_{\Omega_i} > 0$ *for all* $t \geq 0$ *and for some time horizon* $\tau_d > 0$*, ensuring persistence of excitation over the window* $[t - \tau_d, t]$*.*

Proof. Consider the following positive definite Lyapunov function candidate:

$$V(t) = \frac{1}{2} \sum_{i=1}^{n} \left(C_{zi} \hat{e}_i^2(t) + C_{zi} \tilde{e}_i^2(t) + \tilde{\Theta}_i^T(t) \rho_i^{-1} \tilde{\Theta}_i(t) \right). \tag{3.10}$$

Differentiating (3.10) with respect to time yields:

$$\dot{V}(t) = \sum_{i=1}^{n} \left(C_{zi} \hat{e}_i(t) \dot{\hat{e}}_i(t) + C_{zi} \tilde{e}_i(t) \dot{\tilde{e}}_i(t) + \tilde{\Theta}_i^T(t) \rho_i^{-1} \dot{\tilde{\Theta}}_i(t) \right). \tag{3.11}$$

Substituting the error dynamics (3.4)–(3.6) into the first and second terms of (3.11) gives:

$$C_{zi} \hat{e}_i(t) \dot{\hat{e}}_i(t) + C_{zi} \tilde{e}_i(t) \dot{\tilde{e}}_i(t) = -K_{i2} \hat{e}_i^2 - (K_{i1} - K_{i2}) \hat{e}_i e_i + \Delta(P_i) \hat{e}_i - K_{i2} \tilde{e}_i^2 + \tilde{e}_i \tilde{\Theta}_i^T \Phi_i. \tag{3.12}$$

Since $\dot{\tilde{\Theta}}_i = \dot{\hat{\Theta}}_i$, substituting the parameter update law (3.9) into the last term of (3.11) yields:

$$\begin{aligned}\frac{1}{2}\tilde{\Theta}_i^T\rho_i^{-1}\dot{\tilde{\Theta}}_i &= -\tilde{\Theta}_i^T\left(\tilde{e}_i\Phi_i + \epsilon_i\int_{t-\tau_d}^{t}\Phi_i(\sigma)\pi_i(\sigma)d\sigma\right)\\ &= -\tilde{e}_i\tilde{\Theta}_i^T\Phi_i - \epsilon_i\tilde{\Theta}_i^T\left(\int_{t-\tau_d}^{t}\Phi_i(\sigma)\Phi_i^T(\sigma)d\sigma\right)\tilde{\Theta}_i\\ &= -\tilde{e}_i\tilde{\Theta}_i^T\Phi_i - \epsilon_i\tilde{\Theta}_i^T\Omega_i\tilde{\Theta}_i\\ &\le -\tilde{e}_i\tilde{\Theta}_i^T\Phi_i - \epsilon_i\underline{\lambda}_{\Omega_i}\|\tilde{\Theta}_i\|^2.\end{aligned} \tag{3.13}$$

Combining (3.12), (3.13), and (3.11), we obtain:

$$\dot{V} \le \sum_{i=1}^{n}\Big[-K_{i2}\hat{e}_i^2 - (K_{i1}-K_{i2})\hat{e}_ie_i + \Delta(P_i)\hat{e}_i - K_{i2}\tilde{e}_i^2 - \epsilon_i\underline{\lambda}_{\Omega_i}\|\tilde{\Theta}_i\|^2\Big]. \tag{3.14}$$

Grouping terms and applying Young's inequality ($ab \le \frac{a^2}{2} + \frac{b^2}{2}$) to the cross terms $\Delta(P_i)\hat{e}_i$ and $\hat{e}_ie_i$ yields:

$$\Delta(P_i)\hat{e}_i \le \frac{\hat{e}_i^2}{2} + \frac{\bar{\Delta}_i^2}{2}, \tag{3.15}$$

$$\begin{aligned}-(K_{i1}-K_{i2})\hat{e}_ie_i &= -(K_{i1}-K_{i2})\hat{e}_i(\hat{e}_i-\tilde{e}_i)\\ &\le -\frac{K_{i1}-K_{i2}}{2}\hat{e}_i^2 + \frac{K_{i1}-K_{i2}}{2}\tilde{e}_i^2.\end{aligned} \tag{3.16}$$

Substituting (3.15) into the first and second terms of (3.14), one has

$$\dot{V} \le \sum_{i=1}^{n}\Big[-K_{i2}\hat{e}_i^2 - \frac{K_{i1}-K_{i2}}{2}\hat{e}_i^2 - (K_{i2}-\frac{K_{i1}-K_{i2}}{2})\tilde{e}_i^2 - \epsilon_i\underline{\lambda}_{\Omega_i}\|\tilde{\Theta}_i\|^2 + \frac{\bar{\Delta}_i^2}{2}\Big]. \tag{3.17}$$

We selecting controller parameters such that: $K_{i2} > \frac{1}{3}K_{i1} > 0$. Then, we have $\dot{V} \le \sum_{i=1}^{n} -K_{i2}\hat{e}_i^2 - (K_{i2} - \frac{K_{i1}-K_{i2}}{2})\tilde{e}_i^2 + \frac{\bar{\Delta}_i^2}{2}$. According to standard Lyapunov stability theory, this inequality implies that error signals ($\hat{e}_i$ and $\tilde{e}_i$) are bounded and will converge to a compact set. The size of the residual set can be characterized by the parameters κ and d, where $\kappa = \min_i\{K_{i2}, K_{i2} - \frac{K_{i1}-K_{i2}}{2}\}$ and $d = \sum_{i=1}^{n}\frac{1}{2}\bar{\Delta}_i^2$. The size of this residual set can be reduced by increasing the gains K_{i1}, K_{i2}. Using the definition of the prediction error $\tilde{e}_i = \hat{e}_i - e_i$, one has that the tracking error e_i is also small. Then we have that all signals in the closed-loop system are uniformly ultimately bounded, and the tracking error e_i and the prediction error $\tilde{e}_i$ can be driven to a small residual set by an appropriate choice of the controller gains.

Moreover, if the matrix $\Omega_i(t) = \int_{t-\tau_d}^{t}\Phi_i(\tau)\Phi_i^T(\tau)\,d\tau$ satisfies $\lambda_{\min}(\Omega_i(t)) \ge \underline{\lambda}_{\Omega_i} > 0$ for all $t \ge 0$, we have

$$\dot{V} \le -c\left(\sum_{i=1}^{n}\left(e_i^2 + \tilde{e}_i^2 + \|\tilde{\Theta}_i\|^2\right)\right) + d \tag{3.18}$$

where $c = \min_i\{K_{i2} + \frac{K_{i1}-K_{i2}}{2}, K_{i2} - \frac{K_{i1}-K_{i2}}{2}, \epsilon_i\underline{\lambda}_{\Omega_i}\} > 0$. We can conclude that the parameter estimation error $\tilde{\Theta}_i$ can converge to a small neighborhood of 0.

The final, converged parameter values $\bar{\Theta}_i$ are computed by taking the temporal average of $\hat{\Theta}_i(t)$ over a sufficiently long time window $T_a = T_2 - T_1$ once the transients have diminished ($t > T_1$):

$$\bar{\Theta}_i = \frac{1}{T_a}\int_{T_1}^{T_2} \hat{\Theta}_i(\tau)d\tau \tag{3.19}$$

where T_1 and T_2 are the start and end times of the averaging period, respectively. In practice, the averaging window should be selected such that T_1 is large enough to guarantee that the parameter estimates have converged. The endpoint T_2 can be chosen just a few minutes later; the averaging serves only to eliminate any residual small-amplitude oscillations.

This completes the proof. □

Remark 4. *In practice, the interval excitation condition required for parameter convergence is naturally satisfied in multi-zone HVAC systems through three primary mechanisms: (i) Setpoint changes: Zone-specific temperature setpoints often differ and may vary over time, introducing variations in the system dynamics. (ii) Outdoor temperature variations: Diurnal and seasonal fluctuations in outdoor temperature directly influence the regressor $\phi_{i1} = T_{\text{out}} - T_{zi}$, providing continuous excitation. (iii) Occupancy patterns: Variations in internal heat loads due to occupancy schedules affect the lumped parameter θ_{i2} and its associated regressor $\phi_{i2} = 1$, contributing additional richness. Collectively, these factors ensure that the historical data matrix $\Omega_i(t) = \int_{t-\tau_d}^{t} \Phi_i(\tau)\Phi_i^\top(\tau)d\tau$ remains positive definite over moving windows during normal operation.*

3.2. Stage 2: Knowledge-based robust control

3.2.1. Controller design

In Stage 2, we address the scenario where the parameter $\theta_{i2}(t)$ (representing the combined effect of solar heat gain and internal heat load, $\theta_{i2}(t) = A_{\text{win},i}\alpha_{\text{SHGC}}(t)I + Q_{\text{in,s},i}(t)$) becomes time-varying. While we have a fixed nominal estimate $\bar{\theta}_{i2}$ obtained from Stage 1, the actual parameter $\theta_{i2}(t)$ varies with time. The control objective is to track the desired temperature trajectory $T_{zi,d}(t)$ with high performance, despite these time-varying disturbances.

The system dynamics are expressed as:

$$\frac{dT_{zi}}{dt} = \frac{1}{C_{zi}}\left(\bar{\theta}_{i1}\phi_{i1} + \theta_{i2}(t)\phi_{i2} + \sum_{j\in N_i} a_{ij}\bar{\vartheta}_{ij}\varphi_{ij} - E_i\text{sat}(P_i)\right) \tag{3.20}$$

where $\bar{\theta}_{i1}$ and $\bar{\vartheta}_{ij}$ are known parameters identified in Stage 1, while $\theta_{i2}(t)$ is an unknown, bounded, time-varying parameter. We define the time-varying disturbance $d_i(t)$ as the deviation from the nominal value $\bar{\theta}_{i2}$ and other disturbances $\Delta d_i(t)$, such as the identification error in Stage 1:

$$d_i(t) = (\theta_{i2}(t) - \bar{\theta}_{i2})\phi_{i2} + \Delta d_i(t). \tag{3.21}$$

The dynamics can then be rewritten as:

$$\frac{dT_{zi}}{dt} = \frac{1}{C_{zi}}\left(\bar{\theta}_{i1}\phi_{i1} + \bar{\theta}_{i2}\phi_{i2} + \sum_{j\in N_i} a_{ij}\bar{\vartheta}_{ij}\varphi_{ij} - E_i\text{sat}(P_i) + d_i(t)\right). \tag{3.22}$$

Since the disturbance $d_i(t)$ is unknown, we design a disturbance observer to estimate the unknown disturbance $d_i(t)$ in real-time:

$$\begin{cases} \dot{\xi}_i = -\dfrac{L_i}{C_{zi}}\hat{d}_i - \dfrac{L_i}{C_{zi}}\Big(\bar{\theta}_{i1}\phi_{i1} + \bar{\theta}_{i2}\phi_{i2} + \sum\limits_{j\in N_i} a_{ij}\bar{\vartheta}_{ij}\varphi_{ij} - E_i\text{sat}(P_i) - C_{zi}\dot{T}_{zi,d}\Big), \\ \hat{d}_i = \xi_i + L_i e_i \end{cases} \tag{3.23}$$

where $L_i > 0$ is the observer gain, $\hat{d}_i$ is the disturbance estimate, $\tilde{d}_i = d_i - \hat{d}_i$ is the disturbance estimation error, and $e_i = T_{zi} - T_{zi,d}$.

The error dynamics e_i can be obtained as:

$$\dot{e}_i = \frac{1}{C_{zi}}\left[\bar{\theta}_{i1}\phi_{i1} + \bar{\theta}_{i2}\phi_{i2} + \sum_{j\in N_i} a_{ij}\bar{\vartheta}_{ij}\varphi_{ij} - E_i\text{sat}(P_i) + d_i(t) - C_{zi}\dot{T}_{zi,d}\right], \tag{3.24}$$

$$\dot{\hat{d}}_i = \frac{L_i}{C_{zi}}\tilde{d}_i, \tag{3.25}$$

$$\dot{\xi}_i = \dot{\hat{d}}_i - L_i\dot{e}_i = \frac{L_i}{C_{zi}}\tilde{d}_i - L_i\dot{e}_i. \tag{3.26}$$

Substituting the error dynamics (3.24) into (3.26), we have

$$\begin{aligned} \dot{\xi}_i &= \frac{L_i}{C_{zi}}(d_i - \hat{d}_i) - \frac{L_i}{C_{zi}}\left[\bar{\theta}_{i1}\phi_{i1} + \bar{\theta}_{i2}\phi_{i2} + \sum_{j\in N_i} a_{ij}\bar{\vartheta}_{ij}\varphi_{ij} - E_i\text{sat}(P_i) + d_i(t) - C_{zi}\dot{T}_{zi,d}\right] \\ &= -\frac{L_i}{C_{zi}}\hat{d}_i - \frac{L_i}{C_{zi}}\left[\bar{\theta}_{i1}\phi_{i1} + \bar{\theta}_{i2}\phi_{i2} + \sum_{j\in N_i} a_{ij}\bar{\vartheta}_{ij}\varphi_{ij} - E_i\text{sat}(P_i) - C_{zi}\dot{T}_{zi,d}\right]. \end{aligned} \tag{3.27}$$

Design a feedforward-feedback composite control law based on disturbance estimation:

$$P_i = \frac{1}{E_i}\Big(\bar{\theta}_{i1}\phi_{i1} + \bar{\theta}_{i2}\phi_{i2} + \sum_{j\in N_i} a_{ij}\bar{\vartheta}_{ij}\varphi_{ij} - C_{zi}\dot{T}_{zi,d} + K_{i3}e_i + \hat{d}_i\Big) \tag{3.28}$$

where $K_{i3} > 0$ is a feedback gain.

Substituting the control law (3.28) into the error dynamics (3.24):

$$\begin{aligned} \dot{e}_i &= \frac{1}{C_{zi}}\left[\bar{\theta}_{i1}\phi_{i1} + \bar{\theta}_{i2}\phi_{i2} + \sum_{j\in N_i} a_{ij}\bar{\vartheta}_{ij}\varphi_{ij} - E_iP_i + d_i(t) - C_{zi}\dot{T}_{zi,d} + \Delta_i\right] \\ &= \frac{1}{C_{zi}}\left[-K_{i3}e_i + (d_i(t) - \hat{d}_i) + \Delta_i\right] \\ &= \frac{1}{C_{zi}}\left[-K_{i3}e_i + \tilde{d}_i + \Delta_i\right] \end{aligned} \tag{3.29}$$

where $\Delta_i = E_iP_i - E_i\text{sat}(P_i)$ is the error caused by saturation nonlinearity.

The disturbance estimation error dynamics are:

$$\dot{\tilde{d}}_i = \dot{d}_i - \dot{\hat{d}}_i = \dot{d}_i - \frac{L_i}{C_{zi}}\tilde{d}_i. \tag{3.30}$$

Assume the disturbance and its derivative are bounded: $|d_i(t)| \le \bar{d}$, $|\dot{d}_i(t)| \le \bar{d}_m$, and $|\Delta_i| \le \bar{\Delta}_i$.

3.2.2. Stability analysis

Theorem 2. *For system* (3.22)*, under control law* (3.28) *and disturbance observer* (3.23)*, the tracking error e_i and disturbance estimation error $\tilde{d}_i$ are uniformly ultimately bounded. The ultimate bound can be reduced by increasing the controller gain K_{i3} and observer gain L_i.*

Proof. Consider the Lyapunov function:

$$V = \frac{1}{2}C_{zi}e_i^2 + \frac{1}{2}\tilde{d}_i^2. \tag{3.31}$$

Differentiating V:

$$\begin{aligned} \dot{V} &= C_{zi}e_i\dot{e}_i + \tilde{d}_i\dot{\tilde{d}}_i \\ &= e_i(-K_{i3}e_i + \tilde{d}_i + \Delta_i) + \tilde{d}_i(\dot{d}_i - \frac{L_i}{C_{zi}}\tilde{d}_i) \\ &= -K_{i3}e_i^2 + e_i\tilde{d}_i + e_i\Delta_i + \tilde{d}_i\dot{d}_i - \frac{L_i}{C_{zi}}\tilde{d}_i^2. \end{aligned} \tag{3.32}$$

Applying Young's inequality:

$$e_i\tilde{d}_i \le \frac{1}{2\varepsilon_1}e_i^2 + \frac{\varepsilon_1}{2}\tilde{d}_i^2, \tag{3.33}$$

$$e_i\Delta_i \le \frac{1}{2\varepsilon_2}e_i^2 + \frac{\varepsilon_2}{2}\bar{\Delta}_i^2, \tag{3.34}$$

$$\tilde{d}_i\dot{d}_i \le \frac{1}{2\varepsilon_3}\tilde{d}_i^2 + \frac{\varepsilon_3}{2}\bar{d}_m^2. \tag{3.35}$$

Substituting these inequalities:

$$\begin{aligned} \dot{V} &\le -K_{i3}e_i^2 + \left(\frac{1}{2\varepsilon_1}e_i^2 + \frac{\varepsilon_1}{2}\tilde{d}_i^2\right) + \left(\frac{1}{2\varepsilon_2}e_i^2 + \frac{\varepsilon_2}{2}\bar{\Delta}_i^2\right) + \left(\frac{1}{2\varepsilon_3}\tilde{d}_i^2 + \frac{\varepsilon_3}{2}\bar{d}_m^2\right) - \frac{L_i}{C_{zi}}\tilde{d}_i^2 \\ &= -(K_{i3} - \frac{1}{2\varepsilon_1} - \frac{1}{2\varepsilon_2})e_i^2 - \left(\frac{L_i}{C_{zi}} - \frac{\varepsilon_1}{2} - \frac{1}{2\varepsilon_3}\right)\tilde{d}_i^2 + \frac{\varepsilon_3}{2}\bar{d}_m^2 + \frac{\varepsilon_2}{2}\bar{\Delta}_i^2. \end{aligned} \tag{3.36}$$

Choosing $K_{i3} > \frac{1}{2\varepsilon_1} + \frac{1}{2\varepsilon_2}$ and $L_i > C_{zi}(\frac{\varepsilon_1}{2} + \frac{1}{2\varepsilon_3})$, we have:

$$\dot{V} \le -\alpha V + \beta \tag{3.37}$$

where $\alpha = \min\left\{\frac{2(K_{i3}-(\frac{1}{2\varepsilon_1}+\frac{1}{2\varepsilon_2}))}{C_{zi}}, 2(\frac{L_i}{C_{zi}} - (\frac{\varepsilon_1}{2} + \frac{1}{2\varepsilon_3}))\right\}$, $\beta = \frac{\varepsilon_3}{2}\bar{d}_m^2 + \frac{\varepsilon_2}{2}\bar{\Delta}_i^2$. Using Lyapunov stability theory, this inequality implies that the tracking error e_i and disturbance estimation error $\tilde{d}_i$ are uniformly ultimately bounded. The ultimate bound can be reduced by increasing the controller gain K_{i3} and the observer gain L_i.

This completes the proof. □

Remark 5. *Stage 2 builds upon the parameter identification achieved in Stage 1. The disturbance observer effectively estimates and compensates for the time-varying component of $\theta_{i2}(t)$, providing robustness against parameter variations. The proposed scheme leverages the learned parameters $\bar{\theta}_{i1}$ and $\bar{\vartheta}_{ij}$ from Stage 1 while handling uncertainties in $\theta_{i2}(t)$ through disturbance estimation and compensation.*

4. Simulation results

4.1. Four-zone building thermal system simulation

A comprehensive four-zone building thermal system simulation model is developed to validate the proposed two-stage control scheme under realistic operating conditions. The simulation encompasses all major thermal dynamics, including heat transfer through walls and windows, inter-zone thermal interactions, solar radiation effects, and internal heat loads from occupants and equipment. The model parameters, carefully selected to represent a typical commercial building scenario, are systematically presented in Table 2 to provide clear reference for the simulation setup and reproducibility of results. Moreover, the connections between the four regions are established as follows: between Region 1 and Region 2, Region 2 and Region 3, and Region 3 and Region 4. The wall areas corresponding to these connections are 8 m^2, 9 m^2, and 7 m^2, respectively.

Table 2. System parameters for multi-zone building thermal simulation.

Symbol	Value
C_{zi}	[8000, 8000, 8000, 8000] J/°C
U_{wall}	0.8 W/m²°C
U_{wallin}	8 W/m²°C
U_{win}	2.5 W/m²°C
$A_{\text{out},i}$	[15, 12, 18, 11] m²
$A_{\text{win},i}$	[3, 2.5, 4, 3.2] m²
$A_{\text{w},i,j}$	[0, 8, 0, 0, 8, 0, 9, 0, 0, 9, 0, 7, 0, 0, 0, 7] m²
$Q_{\text{in,s},i}$	[250, 200, 300, 230] W
α_{SHGC}	0.75
I	500 W/m²
c	1005 J/kg°C
ρ	1.225 kg/m³
v	1.5 m/s
F	0.2 m²

4.1.1. Stage 1: Concurrent-learning-based adaptive control

The multi-zone temperature control system comprises four interconnected thermal zones with carefully selected parameters to represent realistic building thermal dynamics. In Stage 1, the outdoor temperature is defined as sinusoidal variations $30+5*\sin(2\pi t/7200-\pi/2)$ to mimic realistic summer daytime, all zones initiate from a uniform initial temperature of 25.0°C, and the desired temperature setpoints are strategically set at different values across zones ($T_{z1,d}$ = 24°C, $T_{z2,d}$ = 24.5°C, $T_{z3,d}$ = 25.5°C, $T_{z4,d}$ = 25°C) to demonstrate the controller's capability in maintaining zone-specific comfort requirements while accounting for inter-zone thermal coupling effects and practical actuator constraints. The parameter estimation begins with initial values of $\theta_1(0) = [0, 0, 0, 0]$, $\theta_2(0) = [0, 0, 0, 0]$, and coupling parameters $\vartheta_{ij}(0) = 0$. According to Table 2, the true system parameters, unknown to the controller, can be calculated as $\theta_{1,true} = [388.8, 385.2, 393.7, 386.1]$, $\theta_{2,true} = [1375, 1138, 1800, 1430]$, and $\vartheta_{true} =$

[64, 64, 72, 72, 56, 56]. Control inputs P_i are constrained to [0, 2000], [0, 2000], [0, 2200], [0, 2200]. The parameters are $K_{i1} = 2000$, $K_{i2} = 800$, $\rho_{i1} = 100$, $\rho_{i2} = 200$, $\varrho_{ij} = 400$, and $\epsilon_i = 0.00001$. The historical data terms are collected from $t \in [1s - 101s]$ so that $\Omega_i(t)$ is positive definite.

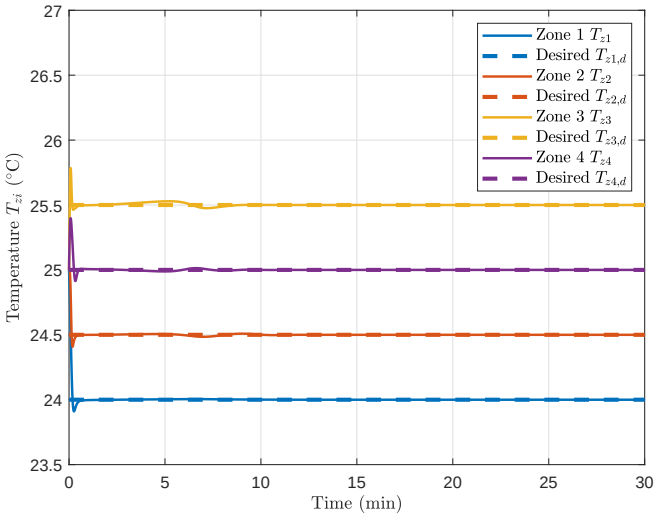

Figure 1. Stage 1: Temperature tracking performance.

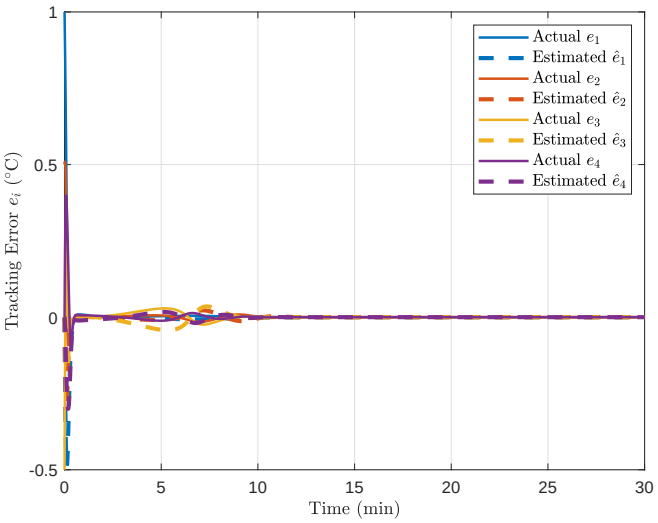

Figure 2. Stage 1: Tracking error and tracking error estimation.

Stage 1 simulation results confirm the efficacy of the proposed adaptive controller. As shown in Figure 1, all four zone temperatures converge to their respective setpoints within 10 minutes with minimal overshoot, indicating satisfactory tracking performance. Figure 2 presents the estimation errors during Stage 1, revealing the precise performance of the error estimation mechanism. The tracking error estimations closely follow the actual tracking errors throughout the simulation, with convergence to near-zero values confirming the accuracy of the estimation algorithm and its integration within the control structure. The control input characteristics during Stage 1 are depicted in Figure 3, showing the power consumption for each zone within the prescribed saturation limits. Through simulation, the minimum eigenvalues $\underline{\lambda}_{\Omega_i}$ of $\Omega_i(t)$ are 0.06, 0.12, 0.22, and 0.20, respectively, which meets the

requirements of Theorem 1 and Remark 4. Figures 4 and 5 demonstrate the parameter estimation performance for θ_{1i} and θ_{2i} parameters, with estimated values converging toward their true values over the 30-minute simulation. The inset provides a detailed visualization of the final 20 minutes, confirming precise parameter identification with minimal estimation error at the steady state. Moreover, time-varying disturbances of the form $20 * \sin(2 * \pi * t/1800 + (i) * \pi/4)$, $i = 1, 2, 3, 4$, are artificially injected into the internal heat load to mimic realistic fluctuations caused by occupancy or equipment usage in Stage 1. Despite these additional disturbances, the parameter estimates θ_{2i} still converged to their true values with high accuracy, as demonstrated in Figure 6, confirming that the update law remains robust even under mild disturbances. Figure 7 presents the coupling parameter ϑ_{ij} estimation results, illustrating effective identification of the thermal interactions between adjacent zones. All six coupling parameters converge to their true values, validating the multi-parameter estimation scheme's ability to capture inter-zone dynamics accurately.

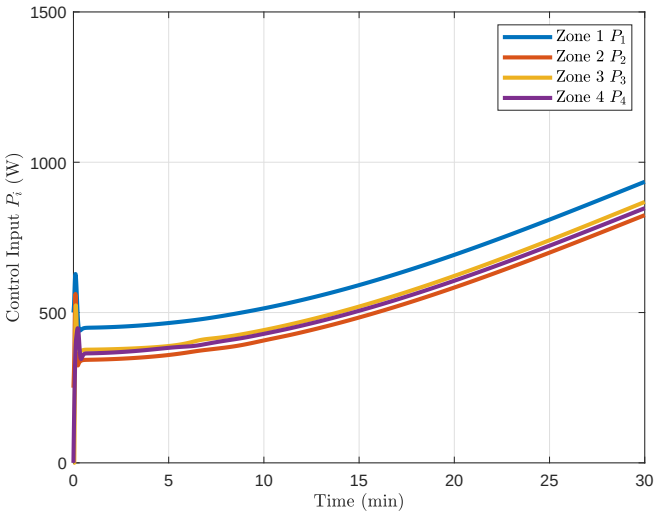

Figure 3. Stage 1: Control input.

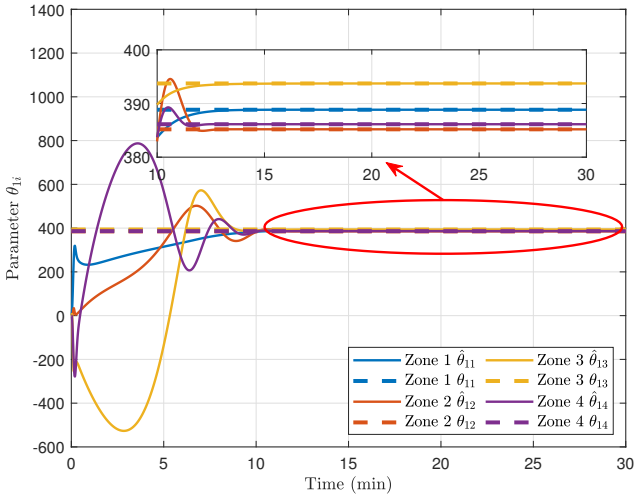

Figure 4. Stage 1: θ_{1i} parameter estimation.

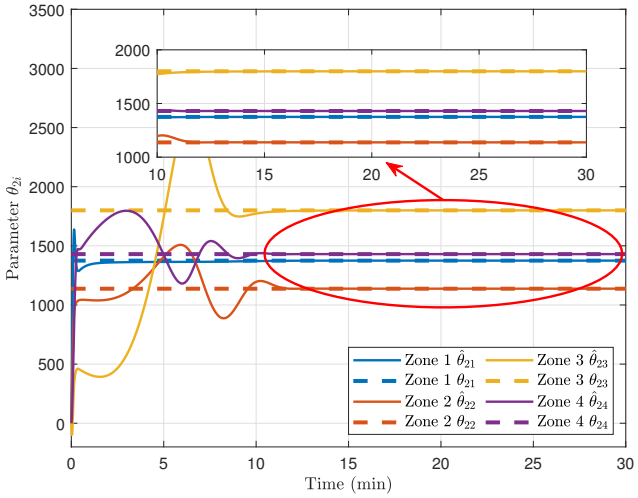

Figure 5. Stage 1: θ_{2i} parameter estimation.

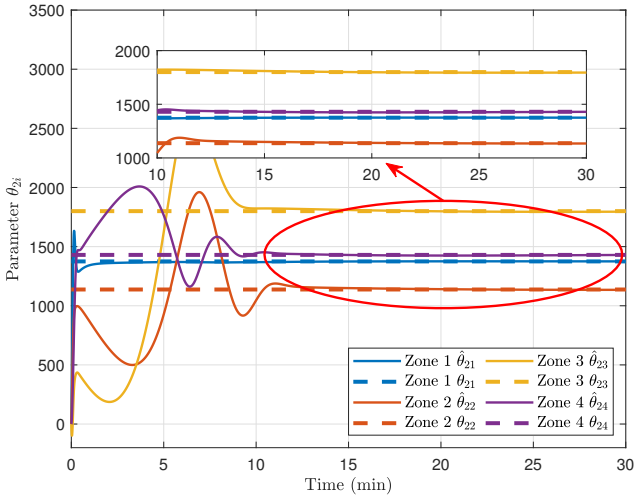

Figure 6. Stage 1: θ_{2i} parameter estimation under disturbances.

To further validate the proposed control framework, a comparative study was conducted using conventional adaptive learning methods [42]. Figure 8 presents the temperature tracking performance of the adaptive learning approach, which demonstrates satisfactory tracking capability with all zones converging to the desired setpoints. This indicates that basic adaptive control can achieve reasonable temperature regulation in the multi-zone system. However, the parameter estimation performance reveals significant limitations of the conventional adaptive approach. Figures 9–11 show the θ_{1i}, θ_{2i}, and ϑ_{ij} parameter estimation results, where the estimated parameters fail to converge to their true values. The estimated parameters exhibit continuous fluctuations without stabilizing to the true parameter values, highlighting the method's inability to provide reliable parameter identification essential for system knowledge acquisition. The comparative results clearly demonstrate that while conventional adaptive learning can achieve satisfactory temperature tracking performance, it fails to ensure parameter

convergence due to the absence of the PE condition. This fundamental limitation prevents the method from truly learning the system knowledge, making it unsuitable for preparing the experience-based control framework required in Stage 2. The proposed method, in contrast, guarantees both performance tracking and parameter convergence, providing a solid foundation for the subsequent disturbance observer-based control phase.

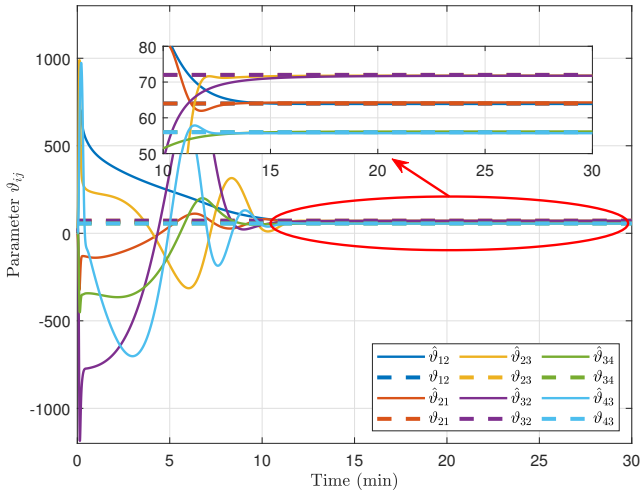

Figure 7. Stage 1: ϑ_{ij} parameter estimation.

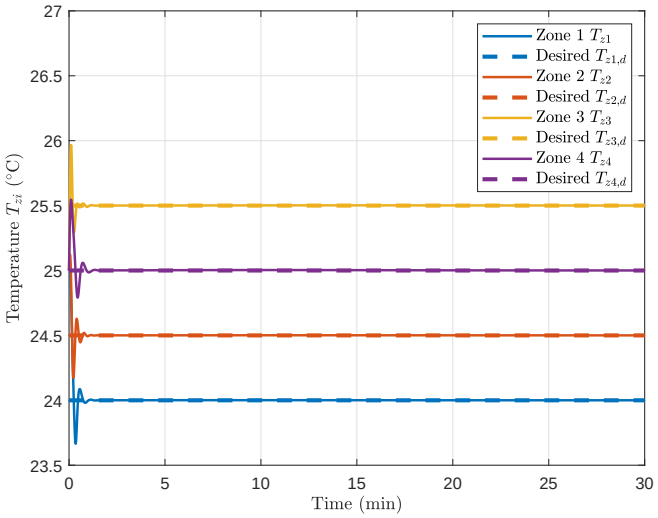

Figure 8. Comparative study [42]: Temperature tracking performance using adaptive learning.

4.1.2. Stage 2: Knowledge-based robust control

The second control stage utilizes the converged parameter estimates obtained from Stage 1 to establish an experience-based control framework. The average parameter values computed during the final third of Stage 1 simulation are employed as fixed parameters in Stage 2: $\bar{\Theta}_i = \frac{1}{10}\int_{20}^{30} \hat{\Theta}_i(\tau)d\tau$. This parameter transfer mechanism enables the controller to leverage the learned system knowledge from Stage 1, forming the foundation for the experience-based control approach. Stage 2 introduces time-varying

external disturbances to evaluate the robustness of the proposed control framework. The disturbances are modeled as sinusoidal functions with different amplitudes and phase shifts for each thermal zone: $d_1(t) = 20\sin\left(\frac{2\pi t}{1800} + \frac{\pi}{4}\right) + 100, d_2(t) = 20\sin\left(\frac{2\pi t}{1800} + \frac{\pi}{2}\right) + 150, d_3(t) = 20\sin\left(\frac{2\pi t}{1800} + \frac{3\pi}{4}\right) + 200, d_4(t) = 20\sin\left(\frac{2\pi t}{1800} + \pi\right) + 250$. In Stage 2, the outdoor temperature profiles are defined as sinusoidal variations $35 + 5 * \sin\left(\frac{2\pi t}{7200} - \frac{\pi}{2}\right)$, all zones are initialized with a uniform initial temperature of 25.0°C, and the desired setpoints are $[25, 24, 24.5, 25.5]$°C for zones 1 through 4, respectively. The parameters are $K_{i3} = 1000$ and $L_i = 500$.

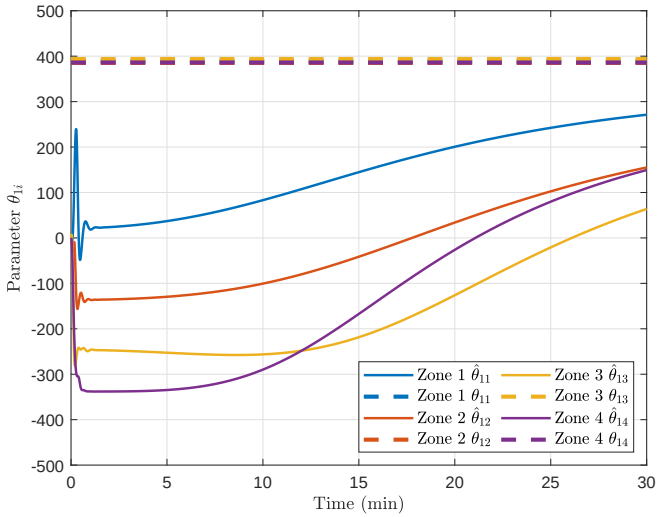

Figure 9. Comparative study [42]: θ_{1i} parameter estimation using adaptive learning.

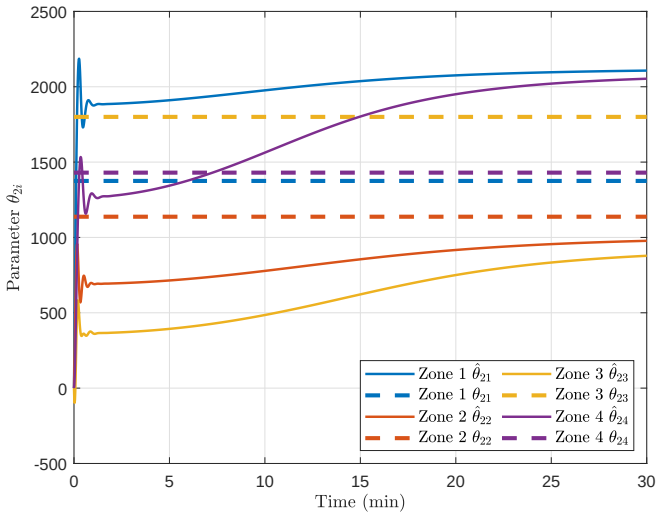

Figure 10. Comparative study [42]: θ_{2i} parameter estimation using adaptive learning.

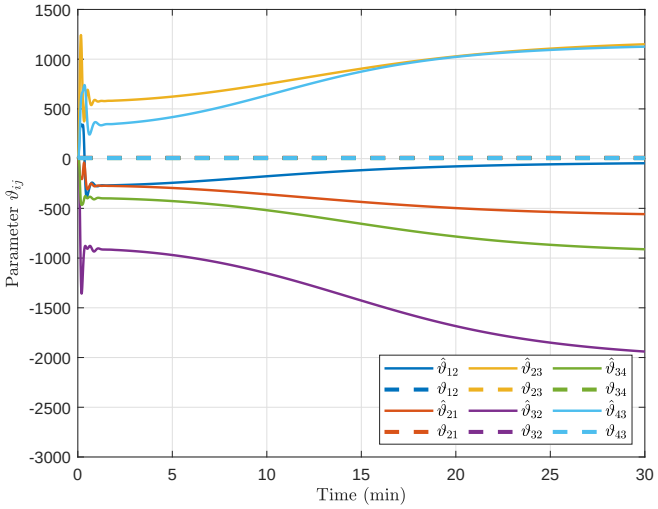

Figure 11. Comparative study [42]: ϑ_{ij} parameter estimation using adaptive learning.

Remark 6. *It should be noted that $\bar{d}$ and $\bar{d}_m$ are only required for the theoretical stability proofs and not needed as parameters in the actual controller. However, bounds $|d_i(t)| \leq \bar{d}$ and $|\dot{d}_i(t)| \leq \bar{d}_m$ can also be conservatively estimated from historical measurements to assist in the selection of parameter L_i, such as peak internal gains, maximal solar irradiance profiles, and building usage schedules. In practice, a larger L_i improves disturbance rejection but increases sensitivity to measurement noise and actuator saturation; hence L_i should be increased until marginal performance gains are small or control effort becomes excessive.*

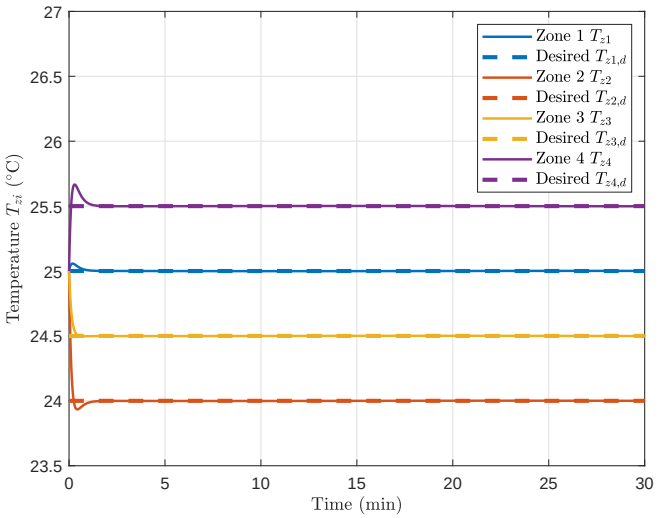

Figure 12. Stage 2: Temperature tracking performance.

Figure 12 displays the temperature tracking performance during Stage 2, maintaining the excellent control characteristics established in Stage 1 while operating under external disturbances. The system demonstrates robust performance with minimal deviation from setpoints, confirming the effectiveness of the disturbance compensation mechanism. Figure 13 evaluates the disturbance observer performance and disturbance errors, demonstrating accurate estimation of the time-varying external disturbances across all

zones. The estimated disturbances closely track the actual disturbances, validating the observer design and its integration within the control framework. The seamless integration of feedforward compensation based on identified parameters and feedback action with disturbance estimation validates the practical effectiveness of the proposed two-stage control architecture for building temperature regulation.

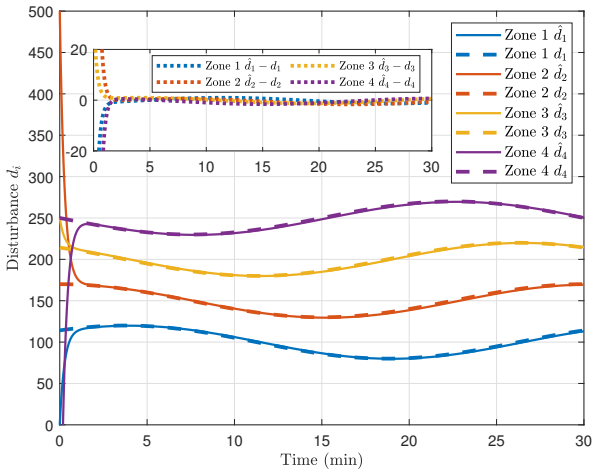

Figure 13. Stage 2: Disturbance observer performance.

4.1.3. Quantitative comparisons

To further demonstrate the advantage of the proposed concurrent learning update law under input saturation, we conduct a quantitative comparison with a conventional concurrent update law by using tracking error [38] under the same saturation constraints. The conventional update law uses the tracking error to update the adaptive parameters. All simulation settings are identical. The following metrics are evaluated for each zone and then averaged: root mean squared error (RMSE) of temperature tracking, computed over the entire simulation horizon (30 min); relative parameter estimation error $\|\tilde{\theta}_1\|_2/\|\theta_1\|_2$ evaluated at the final time (steady-state).

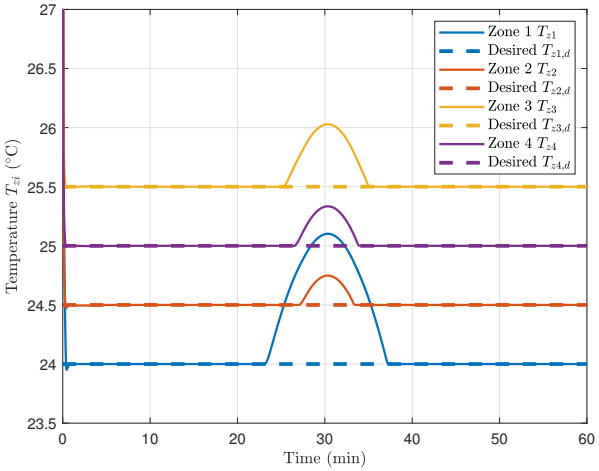

Figure 14. Tracking performance using prediction error.

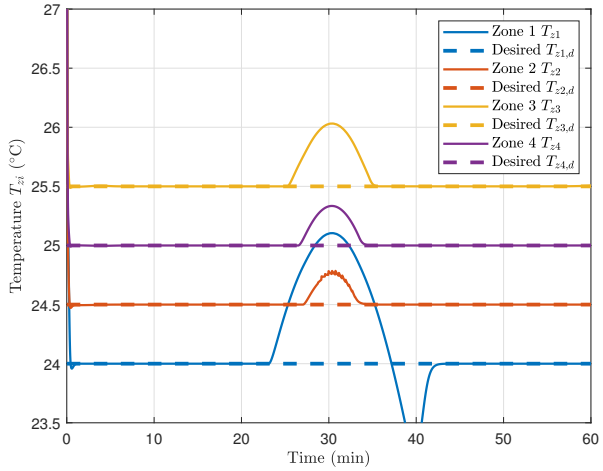

Figure 15. Tracking performance using tracking error.

Figures 14 and 15 compare the tracking errors of the two methods. Both approaches achieve similar transient and steady-state performance. Figures 16 and 17 show the control inputs for both methods. Due to the same saturation limits ($P_{i,\max} = 1500W$), both controllers operate at the saturation boundary during the steady-state. The key difference is revealed in the parameter estimation results, depicted in Figures 18 and 19. The prediction error update law drives all estimated parameters to their true values with high accuracy, despite the presence of saturation. In contrast, the tracking error update law fails to achieve exact convergence. Table 3 summarizes the average results. These results confirm the observation in Remark 3.

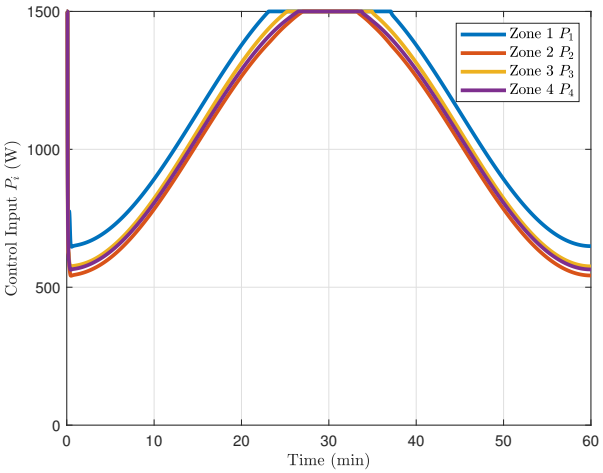

Figure 16. Control input using prediction error.

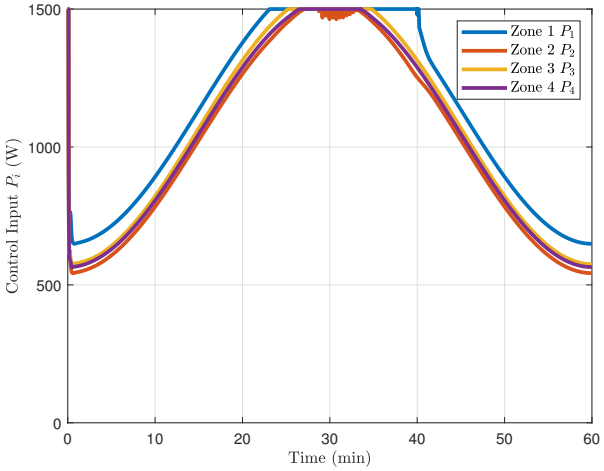

Figure 17. Control input using tracking error.

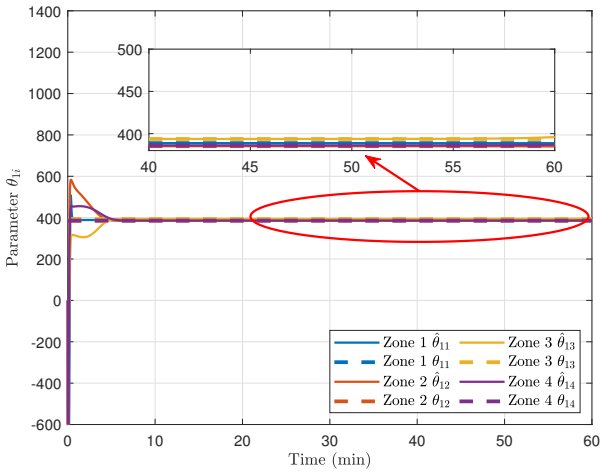

Figure 18. Parameter estimation using prediction error.

Table 3. Quantitative comparison between the proposed and conventional methods [38].

Method	RMSE (°C)	Final $\|\|\tilde{\theta}_1\|\|_2/\|\|\theta_1\|\|_2$
Proposed (Zone 1)	0.41	0.0
Proposed (Zone 2)	0.13	0.0
Proposed (Zone 3)	0.17	0.6
Proposed (Zone 4)	0.13	0.2
Proposed (average)	**0.21**	**0.2**
Conventional (Zone 1)	0.43	0.0
Conventional (Zone 2)	0.13	0.0
Conventional (Zone 3)	0.17	26.4
Conventional (Zone 4)	0.13	0.4
Conventional (average)	**0.22**	**6.7**

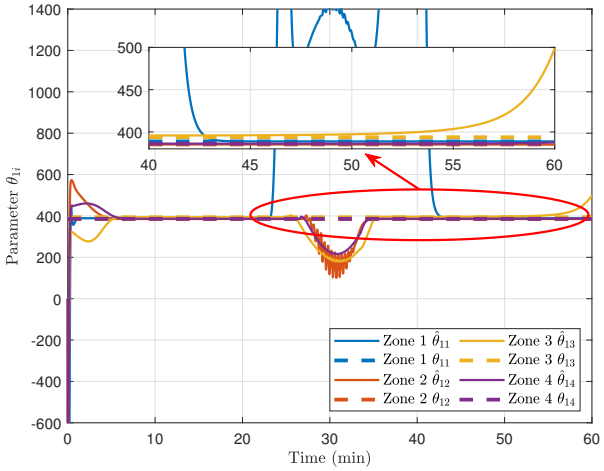

Figure 19. Parameter estimation using tracking error.

4.2. Extension to a 12-zone building

To further evaluate the scalability of the proposed two-stage framework, we consider a larger 12-zone building model with randomly generated thermal parameters and interconnection topology. The simulation settings are analogous to those in the four-zone case, with zone-specific desired temperatures ranging from 24°C to 26.2°C.

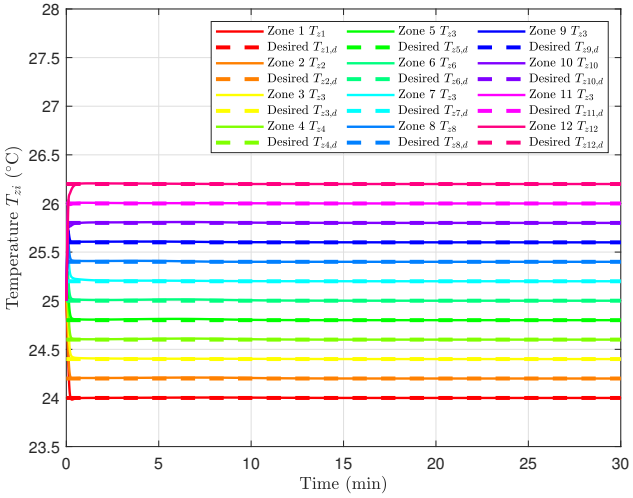

Figure 20. Stage 1: Temperature tracking performance of the 12-zone building.

Figure 20 shows the small temperature tracking errors for 12 zones during Stage 1. In Stage 2, time-varying disturbances $d_i(t) = A_i \sin(2\pi t/1800) + B_i$ with random amplitudes $A_i \in [10, 30]$ and biases $B_i \in [0, 300]$ are applied. As illustrated in Figure 21, the disturbance observer-based controller maintains small tracking errors. The computational cost mainly comes from parameter adaptation and disturbance observers, which is acceptable for real-time building control systems. Since only neighborhood information exchange is required, the communication load is low. The modular and

distributed structure allows further extension to larger-scale multi-zone buildings with acceptable complexity increments.

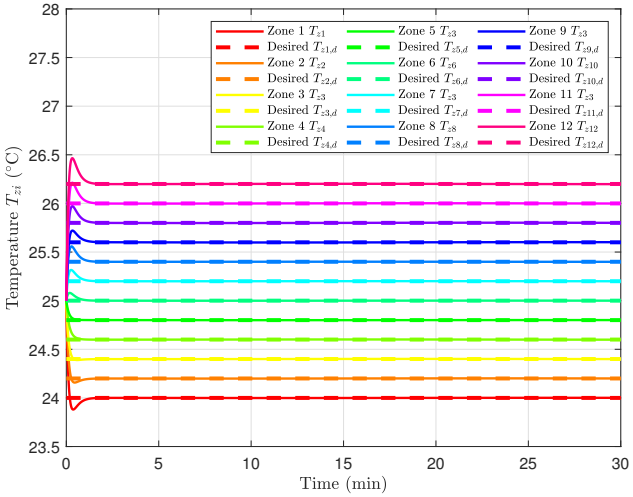

Figure 21. Stage 2: Temperature tracking performance of the 12-zone building.

5. Conclusions

This paper proposes a bio-inspired two-stage learning control framework for multi-zone building thermal systems with unknown parameters and time-varying disturbances, mimicking the "learning-reusing" paradigm observed in biological systems. In the first stage, a concurrent-learning-based adaptive control scheme successfully identifies the unknown system parameters without requiring persistent excitation, ensuring parameter convergence through the utilization of recorded data. The second stage leverages the identified knowledge to construct a disturbance observer-based robust controller, which effectively compensates for time-varying disturbances and model uncertainties. The proposed control strategy offers a practical and efficient solution for intelligent building energy management. Future work will extend this framework to explicitly incorporate thermal comfort metrics [28] and energy optimization [29, 30] into the control objectives, and explore data-driven intelligent networked control schemes [19, 40] to enhance scalability and interconnectivity in large-scale building automation systems.

Use of AI tools declaration

The authors declare they have not used Artificial Intelligence (AI) tools in the creation of this article.

Acknowledgments

This work was supported in part by the Open Project of Key Laboratory of Marine Environmental Survey Technology and Application, Ministry of Natural Resources under Grant MESTA-2024-A002, in part by the National Natural Science Foundation of China (NSFC) under Grant 62403155, and in part by the Research Start-up Foundation of Nanjing Normal University, Natural Science Foundation of Higher Education Institutions in Jiangsu Province, under Grant 23KJB470021.

Conflict of interest

The authors declare there are no conflicts of interest.

References

1. N. Asim, M. Badiei, M. Mohammad, H. Razali, A. Rajabi, L. C. Haw, et al., Sustainability of heating, ventilation and air-conditioning (HVAC) systems in buildings-An overview, *Int. J. Environ. Res. Public Health*, **19** (2022), 1016. https://doi.org/10.3390/ijerph19021016
2. X. Wang, Y. Bai, Z. Li, W. Zhao, S. Ding, Observer-based event triggering security load frequency control for power systems involving air conditioning loads, *Electron. Res. Arch.*, **32** (2024), 6258–6275. https://doi.org/10.3934/era.2024291
3. S. Sierla, H. Ihasalo, V. Vyatkin, A review of reinforcement learning applications to control of heating, ventilation and air conditioning systems, *Energies*, **15** (2022), 3526. https://doi.org/10.3390/en15103526
4. S. Taheri, P. Hosseini, A. Razban, Model predictive control of heating, ventilation, and air conditioning (HVAC) systems: A state-of-the-art review, *J. Build. Eng.*, **60** (2022), 105067. https://doi.org/10.1016/j.jobe.2022.105067
5. A. Afram, F. Janabi-Sharifi, Theory and applications of HVAC control systems-A review of model predictive control (MPC), *Build. Environ.*, **72** (2014), 343–355. https://doi.org/10.1016/j.buildenv.2013.11.016
6. G. Serale, M. Fiorentini, A. Capozzoli, D. Bernardini, A. Bemporad, Model predictive control (MPC) for enhancing building and HVAC system energy efficiency: Problem formulation, applications and opportunities, *Energies*, **11** (2018), 631. https://doi.org/10.3390/en11030631
7. B. Tashtoush, M. Molhim, M. Al-Rousan, Dynamic model of an HVAC system for control analysis, *Energy*, **30** (2005), 1729–1745. https://doi.org/10.1016/j.energy.2004.10.004
8. H. Zhao, H. Cui, Y. Zhao, X. Dai, A neural network-based adaptive fault-tolerant cooperation control for multiple trains with unknown parameters, *Electron. Res. Arch.*, **33** (2025), 3931–3949. https://doi.org/10.3934/era.2025174
9. Q. Zhang, M. Mu, H. Ji, Q. Wang, X. Wang, An adaptive type-2 fuzzy sliding mode tracking controller for a robotic manipulator, *Electron. Res. Arch.*, **31** (2023), 3791–3813. https://doi.org/10.3934/era.2023193
10. M. Shen, T. Zhang, J. H. Park, Q. G. Wang, L. W. Li, Iterative proportional-integral interval estimation of linear discrete-time systems, *IEEE Trans. Autom. Control*, **68** (2023), 4249–4256. https://doi.org/10.1109/TAC.2022.3203226
11. P. Michailidis, I. Michailidis, D. Vamvakas, E. Kosmatopoulos, Model-free HVAC control in buildings: A review, *Energies*, **16** (2023), 7124. https://doi.org/10.3390/en16207124
12. X. Wang, B. Dong, Long-term experimental evaluation and comparison of advanced controls for HVAC systems, *Appl. Energy*, **371** (2024), 123706. https://doi.org/10.1016/j.apenergy.2024.123706

13. X. Xin, Z. Zhang, Y. Zhou, Y. Liu, D. Wang, S. Nan, A comprehensive review of predictive control strategies in heating, ventilation, and air-conditioning (HVAC): Model-free VS model, *J. Build. Eng.*, **94** (2024), 110013. https://doi.org/10.1016/j.jobe.2024.110013

14. M. A. Adesanya, H. Obasekore, A. Rabiu, W. H. Na, Q. O. Ogunlowo, T. D. Akpenpuun, et al., Deep reinforcement learning for PID parameter tuning in greenhouse HVAC system energy optimization: A TRNSYS-Python cosimulation approach, *Expert Syst. Appl.*, **252** (2024), 124126. https://doi.org/10.1016/j.eswa.2024.124126

15. Y. E. Jang, Y. J. Kim, J. P. S. Catalão, Optimal HVAC system operation using online learning of interconnected neural networks, *IEEE Trans. Smart Grid*, **12** (2021), 3030–3042. https://doi.org/10.1109/TSG.2021.3051564

16. J. Cho, Y. Heo, J. W. Moon, An intelligent HVAC control strategy for supplying comfortable and energy-efficient school environment, *Adv. Eng. Inf.*, **55** (2023), 101895. https://doi.org/10.1016/j.aei.2023.101895

17. H. Wang, S. Wang, A disturbance compensation enhanced control strategy of HVAC systems for improved building indoor environment control when providing power grid frequency regulation, *Renewable Energy*, **169** (2021), 1330–1342. https://doi.org/10.1016/j.renene.2021.01.102

18. T. Yu, Z. Zhang, Y. Li, W. Zhao, J. Zhang, Improved active disturbance rejection controller for rotor system of magnetic levitation turbomachinery, *Electron. Res. Arch.*, **31** (2023), 1570–1586. https://doi.org/10.3934/era.2023080

19. M. Shen, X. Wang, J. H. Park, Y. Yi, W. W. Che, Extended disturbance-observer-based data-driven control of networked nonlinear systems with event-triggered output, *IEEE Trans. Syst. Man Cybern. Syst.*, **53** (2023), 3129–3140. https://doi.org/10.1109/TSMC.2022.3222491

20. S. A. A. Rizvi, A. J. Pertzborn, Z. Lin, Reinforcement learning based optimal tracking control under unmeasurable disturbances with application to HVAC systems, *IEEE Trans. Neural Networks Learn. Syst.*, **33** (2022), 7523–7533. https://doi.org/10.1109/TNNLS.2021.3085358

21. N. Nassif, A robust CO_2-based demand-controlled ventilation control strategy for multi-zone HVAC systems, *Energy Build.*, **45** (2012), 72–81. https://doi.org/10.1016/j.enbuild.2011.10.018

22. Y. Zeng, Z. Zhang, A. Kusiak, Predictive modeling and optimization of a multi-zone HVAC system with data mining and firefly algorithms, *Energy*, **86** (2015), 393–402. https://doi.org/10.1016/j.energy.2015.04.045

23. Y. J. Kim, A supervised-learning-based strategy for optimal demand response of an HVAC system in a multi-zone office building, *IEEE Trans. Smart Grid*, **11** (2020), 4212–4226. https://doi.org/10.1109/TSG.2020.2986539

24. S. He, S. L. Dai, Z. Zhao, T. Zou, Y. Ma, UDE-based distributed formation control for MSVs with collision avoidance and connectivity preservation, *IEEE Trans. Ind. Inf.*, **20** (2024), 1476–1487. https://doi.org/10.1109/TII.2023.3274234

25. G. Lymperopoulos, P. Ioannou, Building temperature regulation in a multi-zone HVAC system using distributed adaptive control, *Energy Build.*, **215** (2020), 109825. https://doi.org/10.1016/j.enbuild.2020.109825

26. S. Ma, Y. Zou, S. Li, Coordinated control for air handling unit and variable air volume boxes in multi-zone HVAC system, *J. Process Control*, **107** (2021), 17–26. https://doi.org/10.1016/j.jprocont.2021.09.008

27. C. Cui, J. Xue, L. Liu, Optimal control of HVAC systems through active disturbance rejection control-assisted reinforcement learning, *Energy*, **323** (2025), 135824. https://doi.org/10.1016/j.energy.2025.135824

28. J. Mei, X. Xia, Distributed control for a multi-evaporator air conditioning system, *Control Eng. Pract.*, **90** (2019), 85–100. https://doi.org/10.1016/j.conengprac.2019.06.017

29. G. Chen, H. Zhang, H. Hui, Y. Song, Fast Wasserstein-distance-based distributionally robust chance-constrained power dispatch for multi-zone HVAC systems, *IEEE Trans. Smart Grid*, **12** (2021), 4016–4028. https://doi.org/10.1109/TSG.2021.3076237

30. Q. Jing, Y. Guo, Y. Liu, Y. Wang, C. Du, X. Liu, Optimization study of energy saving control strategy of carbon dioxide heat pump water heater system under the perspective of energy storage, *Appl. Therm. Eng.*, **283** (2025), 129030. https://doi.org/10.1016/j.applthermaleng.2025.129030

31. Y. Liu, C. Cui, A bi-level real-time optimal control strategy for thermal coupled multi-zone dedicated outside air system-assisted HVAC systems, *Energy*, **306** (2024), 132343. https://doi.org/10.1016/j.energy.2024.132343

32. J. Mei, Z. Lu, J. Hu, Y. Fan, Energy-efficient optimal guaranteed cost intermittent-switch control of a direct expansion air conditioning system, *IEEE/CAA J. Autom. Sin.*, **8** (2021), 1852–1866. https://doi.org/10.1109/JAS.2020.1003447

33. H. Zhang, L. Cai, Decentralized nonlinear adaptive control of an HVAC system, *IEEE Trans. Syst. Man Cybern. Part C Appl. Rev.*, **32** (2002), 493–498. https://doi.org/10.1109/TSMCC.2002.807271

34. A. Adegbenro, M. Short, C. Angione, An integrated approach to adaptive control and supervisory optimisation of HVAC control systems for demand response applications, *Energies*, **14** (2021), 2078. https://doi.org/10.3390/en14082078

35. M. A. Abuhussain, B. S. Alotaibi, M. S. Aliero, M. Asif, M. A. Alshenaifi, Y. A. Dodo, Adaptive HVAC system based on fuzzy controller approach, *Appl. Sci.*, **13** (2023), 11354. https://doi.org/10.3390/app132011354

36. C. Wang, D. J. Hill, Learning from neural control, *IEEE Trans. Neural Networks*, **17** (2006), 130–146. https://doi.org/10.1109/TNN.2005.860843

37. Y. Pan, H. Yu, Biomimetic hybrid feedback feedforward neural-network learning control, *IEEE Trans. Neural Networks Learn. Syst.*, **28** (2017), 1481–1487. https://doi.org/10.1109/TNNLS.2016.2527501

38. R. Kamalapurkar, B. Reish, G. Chowdhary, W. E. Dixon, Concurrent learning for parameter estimation using dynamic state-derivative estimators, *IEEE Trans. Autom. Control*, **62** (2017), 3594–3601. https://doi.org/10.1109/TAC.2017.2671343

39. H. Shi, S. He, S. L. Dai, C. Dong, Cooperative learning from neural formation control for uncertain marine surface vehicles with input saturation under switching topology, *IEEE Trans. Transp. Electrif.*, **10** (2024), 7828–7839. https://doi.org/10.1109/TTE.2024.3400366

40. M. Shen, X. Wang, S. Zhu, Z. Wu, T. Huang, Data-driven event-triggered adaptive dynamic programming control for nonlinear systems with input saturation, *IEEE Trans. Cybern.*, **54** (2024), 1178–1188. https://doi.org/10.1109/TCYB.2023.3337779

41. Y. Chen, S. Treado, Development of a simulation platform based on dynamic models for HVAC control analysis, *Energy Build.*, **68** (2014), 376–386. https://doi.org/10.1016/j.enbuild.2013.09.016

42. Y. Jiang, S. Zhu, Q. Xu, B. Yang, X. Guan, Hybrid modeling-based temperature and humidity adaptive control for a multi-zone HVAC system, *Appl. Energy*, **334** (2023), 120622. https://doi.org/10.1016/j.apenergy.2022.120622

AIMS Press